

## Photoinduced Intra- and Intermolecular Energy Transfer in Chlorophyll *a* Dimer

Fulu Zheng, Sebastian Fernandez-Alberti, Sergei Tretiak, and Yang Zhao

*J. Phys. Chem. B*, **Just Accepted Manuscript** • Publication Date (Web): 08 May 2017

Downloaded from <http://pubs.acs.org> on May 14, 2017

### Just Accepted

“Just Accepted” manuscripts have been peer-reviewed and accepted for publication. They are posted online prior to technical editing, formatting for publication and author proofing. The American Chemical Society provides “Just Accepted” as a free service to the research community to expedite the dissemination of scientific material as soon as possible after acceptance. “Just Accepted” manuscripts appear in full in PDF format accompanied by an HTML abstract. “Just Accepted” manuscripts have been fully peer reviewed, but should not be considered the official version of record. They are accessible to all readers and citable by the Digital Object Identifier (DOI®). “Just Accepted” is an optional service offered to authors. Therefore, the “Just Accepted” Web site may not include all articles that will be published in the journal. After a manuscript is technically edited and formatted, it will be removed from the “Just Accepted” Web site and published as an ASAP article. Note that technical editing may introduce minor changes to the manuscript text and/or graphics which could affect content, and all legal disclaimers and ethical guidelines that apply to the journal pertain. ACS cannot be held responsible for errors or consequences arising from the use of information contained in these “Just Accepted” manuscripts.



# Photoinduced Intra- and Intermolecular Energy Transfer in Chlorophyll *a* Dimer

Fulu Zheng,<sup>†</sup> Sebastian Fernandez-Alberti,<sup>\*,‡</sup> Sergei Tretiak,<sup>||</sup> and Yang Zhao<sup>\*,†</sup>

<sup>†</sup> *Division of Materials Science, Nanyang Technological University, Singapore 639798, Singapore,*

<sup>‡</sup> *Universidad Nacional de Quilmes/CONICET, Roque Saenz Peña 352, B1876BXD Bernal, Argentina, and*

<sup>||</sup> *Theoretical Division, Center for Nonlinear Studies (CNLS), and Center for Integrated Nanotechnologies (CINT), Los Alamos National Laboratory, Los Alamos, New Mexico 87545, USA*

E-mail: sfalberti@gmail.com; yzhao@ntu.edu.sg

## Abstract

Applying non-adiabatic excited-state molecular dynamics (NA-ESMD), we investigate excitation energy transfer and exciton localization dynamics in a chlorophyll (Chl) *a* dimer system at the interface of two monomers of light-harvesting complex II (LHCII) trimer. After its optical excitation in the red edge of the Soret (*B*) band, the Chl*a* dimer experiences an ultrafast intra- and intermolecular nonradiative relaxation process to the lowest band ( $Q_y$ ). The energy relaxation is found to run faster in the Chl*a* dimer than in the Chl*a* monomer. Once the molecular system reaches the lowest  $Q_y$  band which is composed of two lowest excited states  $S_1$  and  $S_2$ , the concluding relaxation step involves the  $S_2 \rightarrow S_1$  population transfer, resulting in a relatively slower relaxation rate. The strength of thermal fluctuations exceeds intraband electronic coupling between the states belonging to a certain band ( $B$ ,  $Q_x$ , and  $Q_y$ ), producing localized states on the individual chromophores. Therefore, time evolution of spatial electronic localization during

internal conversion reveals transient trapping on one of the Chl*a* monomers participating in the events of intermonomeric energy exchange. In the phase space domains where electronic states are strongly coupled, these states become nearly degenerate promoting Frenkel-exciton-like delocalization and inter-chromophore energy transfer. As energy relaxation occurs, redistribution of the transition density on two Chl*a* monomers leads to nearly equal distribution of the exciton among the molecules. For a single Chl*a*, our analysis of excitonic dynamics reveals wave function amplitude transfer from the nitrogens and outer carbons to the inner carbon atoms during nonradiative relaxation.

## 1 Introduction

Tasked to harvest solar photons and transform them into chemical energy with extremely high efficiency, photosynthesis is an essential biological process on the Earth. In natural photosynthetic systems, photons are absorbed by the light-harvesting complexes (LHCs) and excitation energy is then transferred to reaction centers (RCs) where charge separation occurs<sup>1-4</sup>. Tremendous efforts have been devoted to studies of mechanisms underlying natural photosynthesis. A better understanding of the efficient

\*To whom correspondence should be addressed

<sup>†</sup>Nanyang Technological University

<sup>‡</sup>Universidad Nacional de Quilmes/CONICET

<sup>||</sup>Los Alamos National Laboratory

1 energy transfer process also benefits the design  
2 of high fidelity artificial photosynthetic systems  
3 with superior robustness and efficiency.

4 Various photosynthetic species contain  
5 pigment-protein aggregates LHCs, such as  
6 the light-harvesting complex II (LHCII)<sup>5</sup>, the  
7 Fenna-Matthews-Olson (FMO) complex<sup>6-8</sup>,  
8 the light-harvesting complex 1 (LH1)<sup>9</sup> and  
9 the light-harvesting complex 2 (LH2)<sup>10,11</sup>.  
10 Wrapped by proteins, pigments such as chloro-  
11 phylls (Chls), bacteriochlorophylls (Bchls),  
12 carotenoids and phycobilins are functional  
13 molecules for the photon absorption and sub-  
14 sequent excitation energy transfer processes<sup>1,4</sup>.

15 Acting as the main antenna in green plants,  
16 LHCII is the most abundant LHC in nature<sup>5,12</sup>.  
17 LHCII has a trimer structure (shown in Fig.1  
18 (a)) and each monomer contains various pig-  
19 ments, such as Chl*a* and Chl*b*. Solar energy  
20 can be absorbed by both Chl*a* and Chl*b*, and re-  
21 sulting excitation energy is transferred between  
22 the pigments. In addition to intermolecular en-  
23 ergy transfer, the relaxation process from the  
24 high-lying energy excited states to the lowest  
25 excited state is another crucial step in excita-  
26 tion energy transfer in photosynthetic systems.  
27 Extensive efforts have been devoted to study  
28 the internal conversion process in various pho-  
29 tosynthetic pigments, such as Chl*a*<sup>13-17</sup>, Chl*b*<sup>13</sup>,  
30 Bchl*a* and mutants of Bchl*a*<sup>18-20</sup>. However,  
31 only the internal conversion in an individual  
32 pigment is revealed in these investigations<sup>13-20</sup>.  
33 A pigment dimer is an ideal model to study the  
34 intermolecular energy transfer and the internal  
35 conversion details simultaneously.

36 Upon photoexcitation, nonradiative relax-  
37 ation occurs from high-lying energy excited  
38 states to the lowest excited state of pigments in  
39 photosynthetic pigment-protein complexes. As  
40 one of the key processes in the first step of pho-  
41 tosynthesis, nonradiative relaxation in the sin-  
42 gle Chl*a* and Chl*b* molecules<sup>13,14</sup> has been stud-  
43 ied with the nonadiabatic excited-state molec-  
44 ular dynamics (NA-ESMD)<sup>21,22</sup>. The ratio  
45 of simulated relaxation constants in Chl*a* and  
46 Chl*b* monomers agreed well with that from ul-  
47 trafast transient absorption spectroscopy. This  
48 approach has also been successfully applied to  
49 study ultrafast intramolecular exciton redistri-

50 bution and energy relaxation after excitation in  
51 large-scale organic conjugated molecules<sup>22-26</sup>.  
52 In photosynthesis, intermolecular excitation en-  
53 ergy relaxation is critical to energy transfer in  
54 photosynthetic systems since many pigments  
55 can be excited simultaneously and are partic-  
56 ipating in the global energy flux. We extend  
57 our investigations to the inter-pigment energy  
58 transfer, a fundamental process for the energy  
59 transfer in LHCs. In this work we apply the  
60 NA-ESMD method to investigate the energy  
transfer in Chl*a* dimer (shown in Fig.1 (b)) sys-  
tem.

The rest of the paper is organized as fol-  
lows. The NA-ESMD methodology and compu-  
tational details are described in Section 2. Sim-  
ulation results and discussions are presented in  
Section 3 including population dynamics, en-  
ergy relaxation pathways, and inter- and intra-  
monomer energy transfer in Chl*a* dimer. Con-  
clusions are drawn in Section 4.

## 2 Theoretical and Computa- tional Details

### 2.1 NA-ESMD Algorithm

The NA-ESMD algorithm<sup>21,22</sup> is suitable to  
investigate energy relaxation within multiple  
electronic excited states in large-scale organic  
molecules. In this algorithm, classical molecu-  
lar dynamics (MD) is combined with the quan-  
tum transitions approach<sup>27,28</sup> in which excited-  
state energies<sup>29-31</sup>, gradients<sup>32,33</sup>, and non-  
adiabatic coupling terms<sup>21,34-36</sup> are computed  
with “on the fly” analytical calculations. This  
is achieved by applying the collective electron  
oscillator (CEO) method<sup>37-40</sup> with the AM1  
semiempirical Hamiltonian<sup>41,42</sup> at the configu-  
ration interaction singles (CIS) level<sup>43,44</sup>. Ex-  
tensive previous studies have already adopted  
AM1 and similar semiempirical models to in-  
vestigate excited state properties of porphyrin-  
based molecules<sup>23,42,45-54</sup>. The excited states  
calculated with the AM1/CIS method repro-  
duce the measured energy gap between the  
Soret band and the Q<sub>y</sub> band, and has been suc-  
cessfully applied to calculate the excited states

of Chla and Chlb monomers<sup>13,14</sup>. A detailed discussion on the parameter testings, algorithm implementation, the advantages, and various applications of NA-ESMD can be found in the recent literature<sup>21,22,55</sup>.

## 2.2 Simulation Details

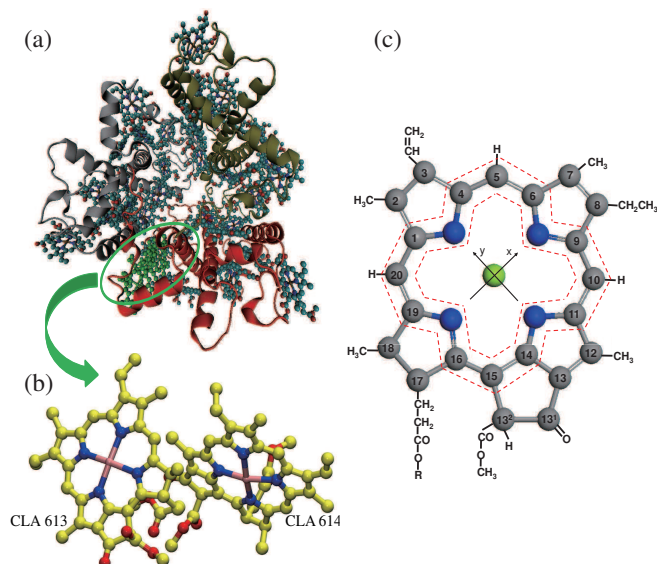


Figure 1: (a) Crystal structure of light-harvesting complex II (LHCII) from *Spinacia oleracea*<sup>5</sup> (PDB ID: 1RWT). (b) The system simulated in this paper, chlorophylla (Chla) dimer in the LHCII complex. (c) Molecular structure of Chla. Carbon (gray) atoms are labeled according to the IUPAC convention for porphyrins, with the standard x- and y- axes of Gouterman’s four-orbital theory shown. The nitrogen and magnesium atoms are in blue and yellow, respectively. Chlorophyll phytyl tails (R) are replaced by a methyl group in the simulations. The total carbon macrocycle is defined as the carbon atoms comprising the porphyrin ring structure (carbon atoms 1 - 20 including atoms C13<sup>1</sup> and C13<sup>2</sup>), whereas the “inner macrocycle” (atoms between two red dashed lines excluding the N atoms) consists of atoms C1, C4, C5, C6, C9, C10, C11, C14, C15, C16, C19, and C20, and the “outer macrocycle” is comprised of carbon atoms from the total carbon macrocycle minus those in the inner macrocycle.

The crystal structure of the LHCII com-

plex in *Spinacia oleracea*<sup>5</sup> (PDB ID: 1RWT) is adopted for our simulation. Two Chla molecules (residues 613 and 614 in chain B of 1RWT) are selected in this work to simulate excited-state dynamics in the Chla dimer system, and the orientation of the two pigments in the dimer is shown in Fig. 1 (b).

First, we perform ground state MD simulation for the Chla dimer from the initial structure for 520 ps at 300 K with a time step of 0.5 fs and four nitrogen atoms of Chla molecules are fixed during the simulation to stabilize the relative molecular configurations in the absence of protein environment. The constant-temperature Langevin equation is adopted to describe the evolution of the nuclear degrees of freedom with a friction coefficient of 2.0 ps<sup>-1</sup>. 500 snapshots from the last 500 ps simulation are extracted with a space of 1 ps, and every snapshot is then used to initialize another set of ground state MD simulation for 200 fs after releasing the constraints on the nitrogen atoms to relax the molecules. The final configurations are used to compute the absorption spectra and to perform the NA-ESMD of the Chla dimer.

The absorption spectrum is calculated for 500 configurations with 20 excited states considered. Shown in Fig. 2 are the entire absorption spectra and the contributions from all the excited states to the spectra. The first absorption band of Chla dimer is around 1.69 eV which is redshifted with respect to the first excited state ( $Q_y$ ) of Chla monomer (1.88 eV) due to interchromophore coupling. The second peak is at about 2.53 eV, and the third, at 2.91 eV close to the Soret band of the Chla monomer. As it has been pointed out previously<sup>13</sup>, although the absolute excitation energies produced by semiempirical methods deviate from the measurements, energy gaps between excited states agree with experimental findings. This agreement allows simulations to predict the overall timescales of nonradiative relaxation from the high-energy excited states in the *B* band to the lowest excited state  $Q_y$  in the Chla monomer, in agreement with transient absorption pump-probe measurements<sup>13</sup>.

A Gaussian-shaped laser pulse is chosen to simulate photo-excitation on the configurations

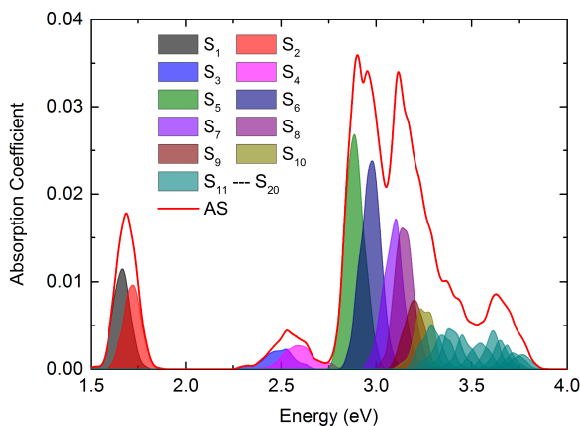


Figure 2: Absorption spectra of Chla dimer. The red solid line is the integral absorption spectra obtained from the sampling results containing 500 molecular configurations. The colored profiles are the contributions of the first 20 excited states considered in the calculations to the final absorption spectra. The contributions of  $S_{11} - S_{20}$  are represented with gray profiles.

obtained from the ground state MD. Excited state  $\alpha$  is initially populated according to a Frank-Condon window defined by  $g_{\alpha}(\mathbf{r}; \mathbf{R}) = (f_{\alpha}/\Omega_{\alpha}^2) \exp[-T^2(E_{\text{laser}} - \Omega_{\alpha})^2]$  where  $f_{\alpha}$  is the normalized oscillator strength of state  $\alpha$  with a frequency of  $\Omega_{\alpha}$ ,  $\mathbf{r}(\mathbf{R})$  is the electronic (nuclear) coordinate, and  $E_{\text{laser}}$  is the laser energy. In this study, the Gaussian-shaped laser pulse is centered at 2.93 eV (423 nm) with a standard deviation of 42.5 fs corresponding to a full width at half maximum (FWHM) of 100 fs. A total of 500 independent excited state trajectories are calculated for 1 ps at 300 K, with a classical time-step of  $\Delta t = 0.1$  fs and  $N_q = 4$  quantum time steps per classical step to simultaneously propagate the coefficients of the electronic states. During the excited state dynamics, the 10 lowest excited states are taken into account for each trajectory.

## 2.3 Electronic Transition Density Analysis

To study the exciton delocalization over the Chla dimer, the electronic transition density

(TD) is calculated as

$$(\rho^{g\alpha})_{nm} \equiv \langle \phi_{\alpha}(\mathbf{r}; \mathbf{R}(t)) | c_m^{\dagger} c_n | \phi_g(\mathbf{r}; \mathbf{R}(t)) \rangle \quad (1)$$

where  $\phi_g(\mathbf{r}; \mathbf{R}(t))$  ( $\phi_{\alpha}(\mathbf{r}; \mathbf{R}(t))$ ) is the wave function of the AM1/CIS adiabatic ground (excited) state,  $c_m^{\dagger}$  ( $c_n$ ) are the creation (annihilation) operators, and indices  $n$  and  $m$  refer to the atomic orbital basis functions. The diagonal elements  $(\rho^{g\alpha})_{nn}$  represent the net change of the electronic density resulting from excitation from the ground state  $g$  to an electronic excited state  $\alpha$ <sup>56</sup>. The normalization condition  $\sum_{n,m} (\rho^{g\alpha})_{nm}^2 = 1$  is valid within the CIS approximation<sup>31</sup>. The fraction of the TD localized on different Chla monomers, or arbitrary groups of atoms in the pigment can be obtained by summing up the atomic contributions belonging to each of them as

$$(\rho^{g\alpha})_X^2 = \sum_{n_A, m_A} (\rho^{g\alpha})_{n_A, m_A}^2 + \frac{1}{2} \sum_{n_B, m_B} (\rho^{g\alpha})_{n_B, m_B}^2 \quad (2)$$

where A is the index of atoms localized in the X-group, and the index B labels the atoms located at the interface of group X and another group.

## 3 Results and Discussions

### 3.1 Population Dynamics

To investigate internal conversion dynamics in the Chla dimer, we compute the average classical populations of the electronic states from the ensemble of 500 trajectories. The average populations for the first six excited states are shown in Fig. 3. Here we can clearly see that near 90% of the excitation relaxes to the lowest excited states within 600 fs.

According to the simulated absorption spectra of the Chla dimer, we categorize the first ten excited states in our simulations into three bands, i.e.,  $Q_y$ ,  $Q_x$  and  $B$  bands. The  $S_1$  and  $S_2$  states yield the  $Q_y$  band while the  $S_3$  and  $S_4$  states contribute to the  $Q_x$  band. The  $B$  band is composed of excited states  $S_5 - S_{10}$ . The average populations for these three bands are computed by summing the average populations of corresponding electronic states which belong

to the bands.

To quantify the internal conversion rates in the Chla dimer, we adopt a first-order mono-directional transfer model from  $B$  to  $Q_x$  and from  $Q_x$  to  $Q_y$  with rate constants  $k_1$  and  $k_2$ , respectively. This yields the sequential transfer pathway  $B \xrightarrow{k_1} Q_x \xrightarrow{k_2} Q_y$ , to fit the average populations of these three bands.

The population of each band can then be given as

$$B(t) = B_0 e^{-k_1 t} \quad (3)$$

$$X(t) = \frac{k_1 B_0}{k_2 - k_1} (e^{-k_1 t} - e^{-k_2 t}) + X_0 e^{-k_2 t} \quad (4)$$

$$Y(t) = B_0 + X_0 + Y_0 - B(t) - X(t) \quad (5)$$

where  $B_0$ ,  $X_0$ , and  $Y_0$  represent the initial ( $t = 0$ ) populations of the  $B$ ,  $Q_x$ , and  $Q_y$  bands, respectively. The fitting is conducted through a least-squares regression analysis. The rate constants and the corresponding time constants ( $\tau_1 = k_1^{-1}$ ,  $\tau_2 = k_2^{-1}$ ) are presented in Table 1 in comparison to the respective parameters obtained for the Chla monomer<sup>13</sup>. Shown in Fig. 3 (b) are the simulated population on the bands and the fitting results using modeled rate constants. The coefficients of determination ( $R^2$ ) for the population curve fittings are 0.9958, 0.9192, and 0.9985 for  $B(t)$ ,  $X(t)$ , and  $Y(t)$ , respectively.

As shown in Table 1, the  $B \rightarrow Q_x$  relaxation is marginally slower in the Chla dimer than that in the Chla monomer. In stark contrast, the dimer system has much faster  $Q_x \rightarrow Q_y$  transfer rate compared to the Chla monomer. Consequently, the overall relaxation from  $B$  to  $Q_y$  in the Chla dimer (142 fs) is faster than that in the Chla monomer (227 fs). For the Chla dimer, each of the three energy bands is mainly composed of two electronic states as shown in Fig. 2. As a result of the intermolecular electronic coupling and the configurational differences between the two monomers, there is a level splitting between the two electronic states (the so-called Davydov's pair) comprising the energy band of the Chla dimer. The level splitting reduces the effective energy gaps between the absorption peaks of the Chla dimer and enhances the relaxation efficiency between these

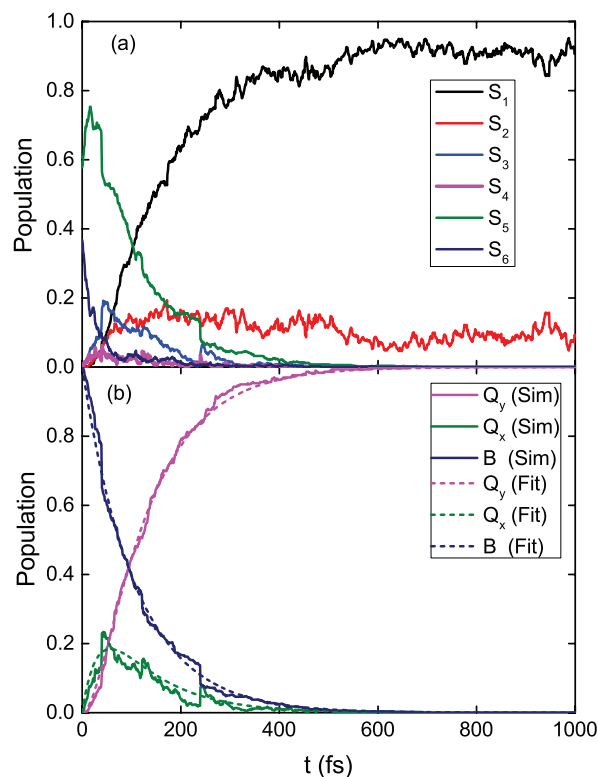


Figure 3: Calculated time evolution of classical population for (a) the lowest six electronic states and (b) three bands of Chla dimer system. The results are averaged over 500 trajectories. Dashed lines in (b) are the fitting curves of the band populations with the fitting parameters in Table 1.

energy bands.

Once the molecular system reaches the lowest  $Q_y$  band, there is a final relaxation step within it. The population transfer from  $S_2$  to  $S_1$  exhibits contributions from two distinguished energy transfer regimes. As shown in Fig. 3 (a), more than 95% of population transfer to the  $Q_y$  band occurs within 400 fs. In this time interval, the population of  $S_1$  increases quickly as the electronic energy flows into the  $Q_y$  band. From 400 fs on, the energy of  $S_2$  is transferred to  $S_1$  slowly and leads to a gradual increase of the population on  $S_1$ . In order to reveal the fast and slow transfer components from  $S_2$  to  $S_1$ , we fit the population of  $S_1$  using the above model with the transfer rate from  $S_2$  to  $S_1$  being  $k_{S21}$ . It is assumed that in the transfer pathway  $B \xrightarrow{k_1} Q_x \xrightarrow{k_2} S_2 \xrightarrow{k_{S21}} S_1$ , the energy of the  $Q_x$  band is first transferred to  $S_2$  then from  $S_2$  to  $S_1$ . This assumption is based on the fact that

Table 1: Comparison of internal conversion rates obtained from a first-order irreversible population model for  $B \rightarrow Q_x$ ,  $Q_x \rightarrow Q_y$ , and  $B \rightarrow Q_y$  pathways for Chla dimer and monomer<sup>13</sup> systems. Populations of specific excited states are averaged from 500 trajectories for Chla dimer and 500 trajectories for Chla monomer<sup>13</sup> in the NA-ESMD simulations.

System	$B \rightarrow Q_x$		$Q_x \rightarrow Q_y$		$B \rightarrow Q_y$
	$k_1$ (fs <sup>-1</sup> )	$\tau_1$ (fs)	$k_2$ (fs <sup>-1</sup> )	$\tau_2$ (fs)	$\tau_{tot}$ (fs)
Monomer	0.0101	99.2±1.1	0.00781	128±2	227±3
Dimer	0.00924	108.2±1.1	0.02952	33.9±0.7	142±2

only a few hops to  $S_1$  are observed from  $S_5$  (6) and  $S_3$  (29), which are negligible compared to an enormous number of hops from  $S_2$  (3690) to  $S_1$ . Here, the population of  $S_2$  can be fitted by the equation

$$S_2(t) = ae^{-k_1 t} + be^{-k_2 t} + ce^{-k_{S21} t} + S_{20}e^{-k_{S21} t} \quad (6)$$

with

$$a = -\frac{B_0 k_1 k_2}{(k_1 - k_2)(k_{S21} - k_1)},$$

$$b = \frac{B_0 k_1 k_2 + k_1 k_2 X_0 - k_2^2 X_0}{(k_1 - k_2)(k_{S21} - k_2)},$$

and

$$c = \frac{B_0 k_1 k_2 - k_2 k_{S21} X_0 + k_1 k_2 X_0}{(k_{S21} - k_1)(k_{S21} - k_2)}.$$

Subsequently, the population of  $S_1$  is

$$S_1(t) = B_0 + X_0 + S_2(0) + S_1(0) - B(t) - X(t) - S_2(t) \quad (7)$$

We fit the population of  $S_1$  in these two time intervals with Eq. (7) as shown in Fig. 4. By fitting the first 400 fs and subsequent 400-600 fs time-intervals of relaxation dynamics, we obtain the fast  $k_{S21} = 0.0237$  fs<sup>-1</sup> ( $\tau_{S21} = k_{S21}^{-1} = 42.19$  fs) and slow  $k'_{S21} = 0.00716$  fs<sup>-1</sup> ( $\tau'_{S21} = 139.66$  fs) transfer rates, respectively.

### 3.2 Initial Exciton Localization

We analyze exciton localization of various electronic excited states at the moment of Frank-Condon photoexcitation from ground state configurations equilibrated at 300 K. For a certain configuration, a reference monomer is selected as the monomer which has higher fraction of

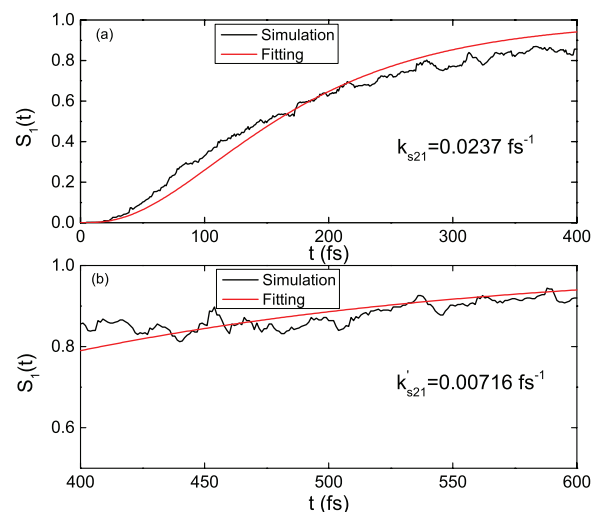


Figure 4: Population of  $S_1$  averaged from 500 trajectories and fitting results with Eq. (7) for fast (a) and slow (b) regimes.

TD of  $S_1$  [ $(\rho^{01})^2_{\text{monomer}} > 0.5$ ] initially, and is denoted as HM of  $S_1$ . Then we obtain the TD distributions of the other states ( $S_2 - S_6$ ) on the reference monomer by constructing histograms of the TD for all initial configurations. Roughly, half of total configurations (i.e., 243 or 48.6% out of 500 configurations) have monomer CLA 613 as their HM of  $S_1$ .

The initial distribution of all the states on the HM of  $S_1$  is shown in Fig. 5. It is clearly seen that  $S_1$  is strongly localized on its HM. The TD of all other electronic states are distributed near 0 and 1 which indicates persistent localization on a single monomer for all cases. As expected, for most configurations,  $S_1$  and  $S_3$  are initially localized on the same monomer while  $S_2$  and  $S_4$  are localized on the other monomer. High-lying energy states  $S_5$  and  $S_6$  seem to be ambiguously localized on any chromophore. Thus, in spite of significant electronic coupling between

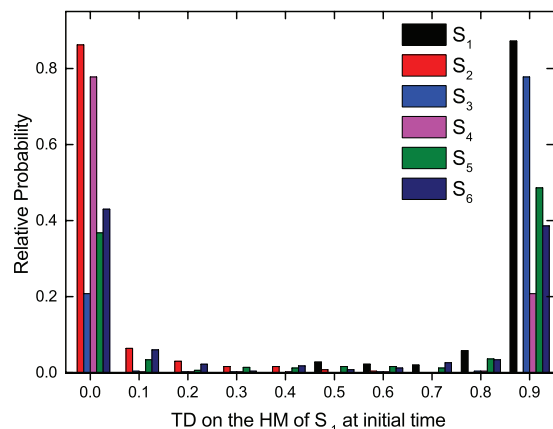


Figure 5: Distribution of the transition density for the electronic states on the higher monomer of  $S_1$  at initial time (500 configurations).

monomers, which splits the electronic states, thermal fluctuations at room temperature essentially localize the excited state wave function initially to a single Chl $a$  in a dimer configuration.

### 3.3 Energy Relaxation Pathways

Subsequent to photoexcitation, the Chl $a$  dimer experiences an efficient Soret ( $B$ ) band  $\rightarrow Q_y$  band energy transition. According to the fewest switches surface hopping (FSSH) algorithm<sup>27</sup> implemented in our NA-ESMD simulations, electronic transitions are described as hops from one initial electronic state  $S_i$  to another  $S_f$  final state. The relative probabilities of effective  $S_i \rightarrow S_f$  transitions during all the NA-ESMD simulations are summarized in Table 2. An effective  $S_i \rightarrow S_f$  transition refers as  $S_i \rightarrow S_f$  hops for which no back-hopping  $S_f \rightarrow S_i$  occurs along the rest time of this NA-ESMD trajectory. The relative probabilities have been normalized for hops corresponding to the same  $S_i$  state.

We can clearly see from the data in Table 2 that the relaxation mainly takes place along the sequential pathway  $S_6 \rightarrow S_5 \rightarrow S_4 \rightarrow S_3 \rightarrow S_2 \rightarrow S_1$  in the Chl $a$  dimer. Transitions from  $S_6$  to  $S_5$ ,  $S_4$  and  $S_3$  occur with relative probabilities of 0.97, 0.02 and 0.01, respectively. According to the ambiguous initial localization of this state (see Fig. 5) these initial relaxation steps involve both intra- and inter- monomer energy

transfer events. In the case of effective hops from  $S_5$ , the sequential pathway to  $S_4$  takes up 78% of its energy transfer flux and, according to Fig. 5, it involves mainly an inter-monomer energy transfer. The intra-monomer  $S_5 \rightarrow S_3$  channel accounts for the remainder 21%. In contrast, effective hops from  $S_4$  mostly develop only through the inter-monomer channel to  $S_3$ . Finally, the inter-monomer channel of  $S_3 \rightarrow S_2$  occupies 95% of the relaxation from that state while the intra-monomer channel holds a minor 5% contribution, followed by a final inter-monomer  $S_2 \rightarrow S_1$  relaxation.

Table 2: Fraction of effective transitions from  $S_i$  to  $S_f$  ( $S_i > S_f$ )

$S_f \backslash S_i$	$S_6$	$S_5$	$S_4$	$S_3$	$S_2$
$S_5$	0.97	-	-	-	-
$S_4$	0.02	0.78	-	-	-
$S_3$	0.01	0.21	1.0	-	-
$S_2$	0	0	0	0.95	-
$S_1$	0	0.01	0	0.05	1.0

### 3.4 Transient Electronic Transition Density Redistribution

Summarizing the above observations, the Soret ( $B$ )  $\rightarrow Q_y$  internal conversion process after photoexcitation of the Chl $a$  dimer takes place mainly through a sequential cascade mechanism involving multiple exciton exchanges between monomers. Notably, a localization pattern shown in Fig. 5 is getting significantly perturbed by the dynamics, i.e., the wave function should not necessarily remain localized on a single Chl $a$ , which is subject to analysis in this section. Namely, the time evolution of the photoinduced inter- and intra- monomer electronic transition can be tracked by TD redistribution in the Chl $a$  dimer. Thus, complementary studies of the exciton spatial localization in the trajectory ensemble reveal a comprehensive picture on the interplay of concomitant inter- and intra-monomer relaxation processes.

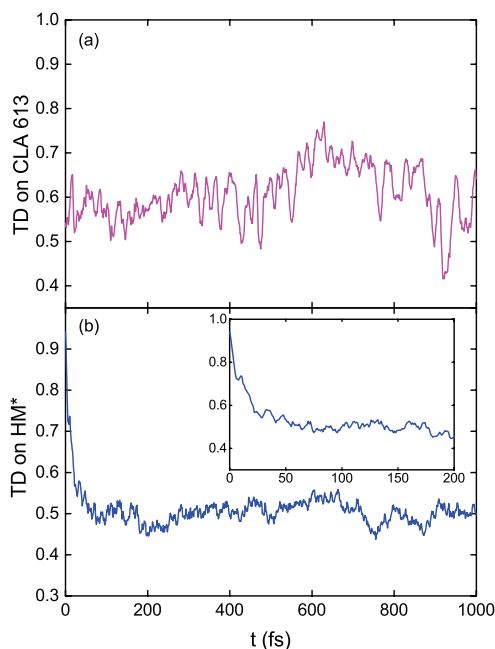


Figure 6: The fraction of electronic transition density localized on (a) the monomer CLA 613 and (b) the higher monomer (HM\*) being averaged over all trajectories.

### 3.4.1 Inter-monomer exciton exchange

The Chla dimer considered in this study is composed of CLA 613 and CLA 614 residues from the chain B of the crystal structure 1RWT of LHCII complex. The laser excitation leads to nearly equivalent probabilities for both residues to become excited initially. In Fig. 6 (a) we show the time evolution of the average fraction of TD on CLA 613  $((\rho^{0\alpha})_{\text{CLA 613}}^2)$ . Its value fluctuates around 0.6, indicating a slightly higher tendency of the exciton to get trapped on it.

In order to further investigate the signatures of the exciton delocalization between both monomers, we define the higher monomer (HM\*) as the monomer with the higher fraction of TD in the current excited state at the initial time,  $(\rho^{0\alpha})_{\text{HM}^*}^2(t=0) > 0.5$ . It is important to stress that, according with the given definition, HM\* can be either CLA 613 or CLA 614 residues and it should be chosen individually for each NA-ESMD trajectory. Once the HM\* has been selected at  $t=0$  for each trajectory, it remains the same throughout this NA-ESMD simulation. The time evolution of the average over all trajectories of  $(\rho^{0\alpha})_{\text{HM}^*}^2$  is depicted in Fig. 6 (b). HM\* corresponds to CLA 613 for

53.6% of trajectories. As a result of an ultrafast effective inter-monomer exciton exchange, the value of  $(\rho^{0\alpha})_{\text{HM}^*}^2$  experiences an ultrafast decrease during the first  $\sim 100$  fs. Its final value of  $\sim 0.5$  may follow from two possible scenarios. In one scenario, a true delocalized electronic state can be equally shared by two monomers, and in the second, it can result from localized states that hop between monomers. In order to distinguish between these scenarios, we further analyze the participation number which is defined as

$$P = \left[ ((\rho^{0\alpha})_{\text{CLA 613}}^2)^2 + ((\rho^{0\alpha})_{\text{CLA 614}}^2)^2 \right]^{-1} \quad (8)$$

where  $(\rho^{0\alpha})_{\text{CLA 613}}^2$  ( $(\rho^{0\alpha})_{\text{CLA 614}}^2$ ) is the fraction of TD localized on monomer CLA 613 (614). The value of  $P$  varies in the interval between 1 and 2 as each monomer is treated as a unit. If  $P \approx 1$ , it means that the TD is almost completely localized on a single Chla monomer, while  $P \approx 2$  means that the TD is delocalized over the two Chla monomers. The time evolution of the average value of  $P$  during the NA-ESMD simulations is shown in Fig. 7. As can be seen, the initial excitation effectively generates a weakly delocalized state between both monomers. Thereafter, the excited state dynamics leads to an almost complete localization of the TD to one monomer within  $\sim 100$  fs.

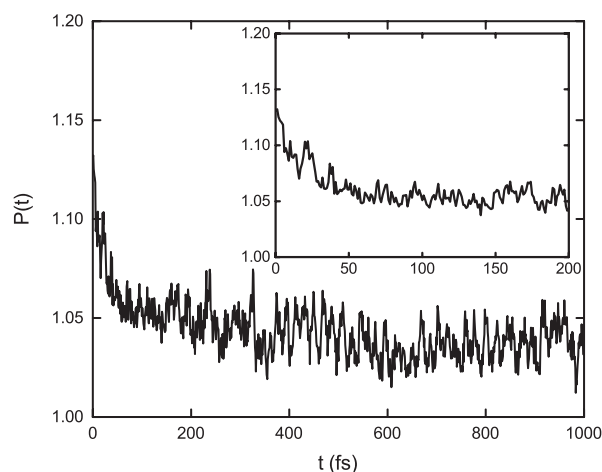


Figure 7: Time evolution of the participation number of Chla dimer taken as an average over all trajectories.

The inter-monomer exciton exchanges

throughout the NA-ESMD simulations can be further analyzed by events with significant changes of  $(\rho^{0\alpha})^2_{\text{monomer}}$ . Figure 8 (a) displays the time dependence of the relative probability of exciton-exchange events between monomers. An event of significant TD exchange between monomers is considered when  $\Delta(\rho^{0\alpha})^2_{\text{monomer}} > 0.5$ . Despite larger probabilities at earlier times, the inter-monomer energy exchange persists throughout the simulations, highlighting the main role of the inter-monomer pathway during the internal conversion process of the Chla dimer. Therefore, an average number of exciton hops between monomers per NA-ESMD simulation is relatively high ( $\sim 38$ ) (see Fig. 8 (b)).

Energy relaxation through localized states on the individual chromophores can be explained by analyzing coupling between states belonging to each band, that is,  $S_1$  and  $S_2$  for  $Q_y$ ,  $S_3$  and  $S_4$  for  $Q_x$ , and  $S_5$  to  $S_{10}$  for  $B$  band. The coupling is computed as half of the energy splitting between two excited states of the Chla dimer, and both the Förster and the Dexter contributions to the coupling can be included<sup>57,58</sup>. This method has been successfully applied to estimate the electronic coupling between the pigments in LH2 (e.g., Ref.<sup>58</sup>). Our calculations on all the 500 initial configurations, obtained from the equilibrated ground state MD simulation, are shown in Table 3. Considering coupling as half of energy splitting between states, we obtained average values of  $224 \text{ cm}^{-1}$  and  $398 \text{ cm}^{-1}$  for  $Q_y$  and  $Q_x$  bands, respectively. Based on the four-orbital model for porphyrins<sup>59,60</sup>, the  $B$  band of chlorophylls are composed of two bands, namely, the  $B_x$  and  $B_y$  bands<sup>61,62</sup>. For the Chla dimer studied in this work, we assign  $S_5$  and  $S_6$  to the  $B_x$  band, and  $S_7$  and  $S_8$  to the  $B_y$  band, respectively. Then we obtain a coupling strength of  $360 \text{ cm}^{-1}$  ( $250 \text{ cm}^{-1}$ ) between the states in  $B_x$  ( $B_y$ ) band. The  $Q_y - Q_y$  and  $B_x - B_x$  coupling strengths computed here agree well with previous results obtained for the LH2 pigments<sup>58</sup>. Compare to the  $Q_y - Q_y$  coupling estimated by the dipole-dipole interaction<sup>63</sup> and the Poisson-TrEsp method<sup>64</sup>, we obtain relatively stronger  $Q_y - Q_y$  coupling in this work as a result of excluding protein en-

vironments. As can be seen, the strength of the thermal fluctuations (FWHM of the excitation energy distribution) do exceed the coupling which leads to localized states on the individual chromophores. Excited state dynamics then separates the states even further due to vibrational relaxation. However, in the phase space domains where electronic states are strongly coupled, states become nearly degenerate promoting delocalization as a Frenkel exciton and facilitating thus efficient inter-chromophore energy transfer.

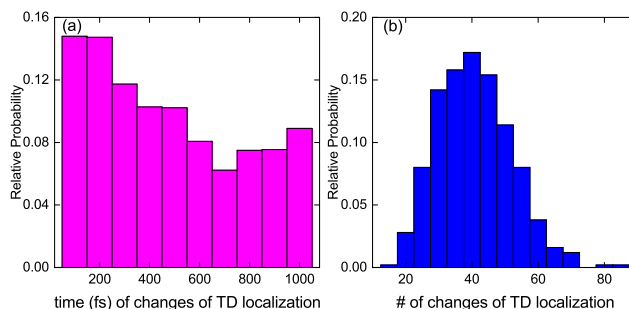


Figure 8: (a) Relative probability of exciton exchange between monomers as a function of time. (b) Histogram of the number of TD localization changes between the monomers during the NA-ESMD simulations.

### 3.4.2 Intra-monomer exciton redistribution

During the internal conversion process of the Chla dimer, each monomer experiences an intramolecular wave function redistribution. We monitor the fractions of TD localized on specific atoms, functional groups, and regions of each Chla monomer. The structure of Chla molecule is depicted in Fig. 1 (c). Following our previous work on the Chla monomer<sup>14</sup>, the porphyrin ring of the molecule is fragmented into following groups, i.e., atom Mg, atoms N, the inner macrocycle and the outer macrocycle. The total carbon macrocycle contains the carbon atoms comprising the porphyrin ring structure (carbon atoms 1 - 20 including atoms C13<sup>1</sup> and C13<sup>2</sup>). The “inner macrocycle” (atoms between two red dashed lines excluding the N atoms in Fig. 1 (c)) is comprised of atoms C1,

Table 3: Average excitation energy and Full width at half maximum (FWHM) extracted from the Gaussian fitting of the excitation energy distribution from 500 configurations.

band	excited state	average excitation energy (eV)	FWHM (eV)
$Q_y$	1	1.669	0.104
	2	1.725	0.101
$Q_x$	3	2.478	0.177
	4	2.577	0.173
$B$	5	2.889	0.116
	6	2.978	0.120
	7	3.094	0.136
	8	3.156	0.111
	9	3.207	0.114
	10	3.252	0.117

C4, C5, C6, C9, C10, C11, C14, C15, C16, C19, and C20. The “outer macrocycle” consists of carbon atoms in the total carbon macrocycle excluding those in the inner macrocycle.

For each trajectory, we denote the HM\* (LM\*) as the monomer which has higher (lower) fraction of TD in the current excited state initially. We depict the time evolution of the averaged TD localized on each partition of the porphyrin ring of either HM\* and LM\* in Fig. 9 (a)-(d). Within  $\sim 100$  fs, the fractions of TD on specific atoms (Mg and N atoms), and regions (inner and outer carbon macrocycles) of LM\* approach to those of HM\*. The overall redistribution behavior of the TD on a monomer during the conversion from  $B$  to  $Q_y$  is analyzed and depicted in Fig. 9 (e). The intramolecular exciton redistribution within each monomer of the Chla dimer reproduces previous results observed for individual Chla molecule<sup>14</sup>. That is, the overall  $B \rightarrow Q_y$  energy relaxation process implies the transfer of localized TD from the N atoms and the outer carbon macrocycle to the inner carbon macrocycle, and the central Mg atoms play minor roles in the exciton relocalization.

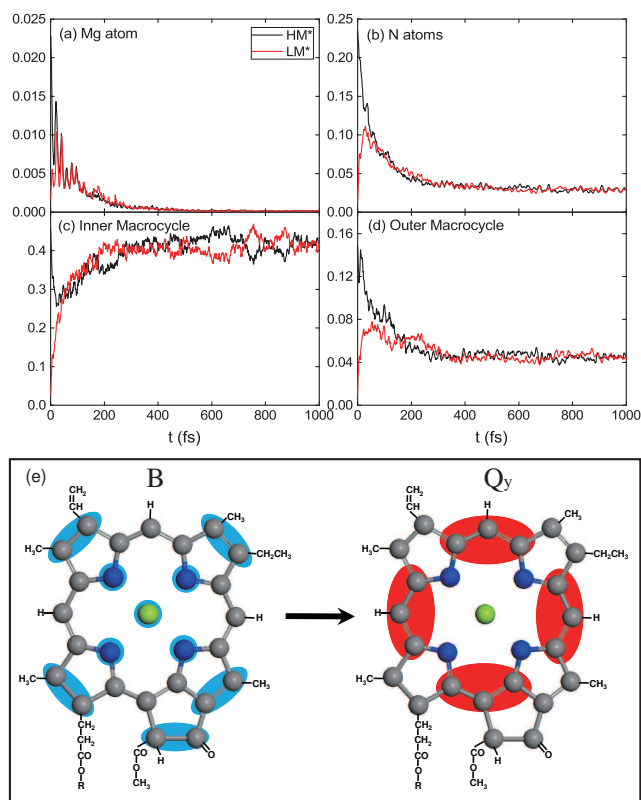


Figure 9: The time evolution of the averaged TD localized on the (a) Mg atom, (b) N atoms, (c) inner macrocycle, and (d) outer macrocycle for higher monomer (HM\*) and lower monomer (LM\*). (e) Schematic representation for the predominant transition density redistribution on a chlorophyll *a* monomer during the conversion from  $B$  to  $Q_y$ . Background areas with blue and red colors represent the transition density for the  $B$  and  $Q_y$  bands, respectively.

## 4 Conclusions

Electronic dynamics simulations beyond the Born-Oppenheimer approximation have been carried out to investigate photoinduced intra- and inter- chromophore energy transfer in a Chla dimer at the interface of two units of light-harvesting complex II (LHCII) trimer from *Spinacia oleracea*<sup>5</sup>. We observe the overall Soret ( $B$ )  $\rightarrow$   $Q_y$  internal conversion in a Chla dimer to be faster than that in an isolated Chla monomer. Indeed, dimerization induced energy level splittings in a molecular pair effectively reduce the energy gaps between the excited states and ultimately lead to a faster relaxation rate compared to a single chro-

1 mophore. Our analysis of electronic transi-  
2 tion density dynamics signified by its redi-  
3 stribution in the Chla dimer, reveals compe-  
4 tition between concomitant inter- and intra-  
5 monomer relaxation processes. The initial laser  
6 excitation generates a weakly delocalized state.  
7 The strength of thermal fluctuations gener-  
8 ally exceeds electronic coupling between states,  
9 leading to quasi-localized states on the indi-  
10 vidual chromophores. The excited state dy-  
11 namics triggers vibrational relaxation and a  
12 complete state localization. However, in the  
13 phase space domains where electronic states are  
14 strongly coupled, states become nearly degener-  
15 ate promoting exciton delocalization and facili-  
16 tating efficient inter-chromophore energy trans-  
17 fer. The internal conversion process proceeds  
18 mainly through a sequential-cascade pathway  
19  $S_6 \rightarrow \dots \rightarrow S_1$  involving multiple exciton ex-  
20 changes between monomers. Once the molec-  
21 ular system reaches the lowest  $Q_y$  band, the  
22 final  $S_2 \rightarrow S_1$  relaxation step takes signifi-  
23 cantly longer time. The inter-molecular en-  
24 ergy exchange still persists throughout the en-  
25 tire 1 ps dynamics, highlighting the main role  
26 of the inter-monomer pathway during the in-  
27 ternal conversion process in the Chla dimer.  
28 As non-radiative relaxation develops, energy  
29 redistribution on two Chla molecules leads to  
30 nearly equal distribution of the exciton among  
31 the monomers due to incoherent exciton hop-  
32 ping between localized excited states. De-  
33 spite the inter-monomer exciton exchanges, the  
34 intra-molecular exciton redistribution within  
35 each monomer of the Chla dimer reproduces  
36 previous results observed for individual Chla  
37 molecules<sup>14</sup>.

## 48 Acknowledgement

49 One of the authors (F.Z.) would like to thank  
50 Prathamesh Shenai for helpful discussion. The  
51 authors acknowledge support from Singapore  
52 National Research Foundation through the  
53 Competitive Research Programme (CRP) un-  
54 der Project No. NRF-CRP5-2009-04. Sup-  
55 port from the Singapore Ministry of Educa-  
56 tion Academic Research Fund Tier 1 (Grant

No. RG106/15) is also gratefully acknowl-  
57 edged. S.T. acknowledges support from the  
58 Center for Integrated Nanotechnology (CINT),  
59 a U.S. Department of Energy, Office of Basic  
60 Energy Sciences user facility (under contract  
DE-AC52-06NA25396). S.F.A is supported in  
part by CONICET, UNQ, ANPCyT (PICT-  
2014-2662).

## References

- (1) Blankenship, R. E. *Molecular Mechanisms of Photosynthesis*; Blackwell Publishing: Williston, VT, USA, 2002.
- (2) Croce, R.; van Amerongen, H. Natural Strategies for Photosynthetic Light Harvesting. *Nat. Chem. Bio.* **2014**, *10*, 492-501.
- (3) Scholes, G. D.; Fleming, G. R.; Olaya-Castro, A.; van Grondelle, R. Lessons from Nature about Solar Light Harvesting. *Nat. Chem.* **2011**, *3*, 763-774.
- (4) Rabinowitch, E.; Govindjee. *Photosynthesis*; Wiley: New York, 1969.
- (5) Liu, Z.; Yan, H.; Wang, K.; Kuang, T.; Zhang, J.; Gui, L.; An X.; Chang, W. Crystal Structure of Spinach Major Lightharvesting Complex at 2.72 Å Resolution. *Nature* **2004**, *428*, 287-292.
- (6) Fenna, R. E.; Matthews, B. W. Chlorophyll Arrangement in a Bacteriochlorophyll Protein from *Chlorobium limicola*. *Nature* **1975**, *258*, 573-577.
- (7) Li, Y. F.; Zhou, W. L.; Blankenship, R. E.; Allen, J. P. Crystal Structure of the Bacteriochlorophyll a Protein from *Chlorobium tepidum*. *J. Mol. Biol.* **1997**, *271*, 456-471.
- (8) Camara-Artigas, A.; Blankenship, R. E.; Allen, J. P. The Structure of the FMO Protein from *Chlorobium tepidum* at 2.2 Angstrom Resolution. *Photosynth. Res.* **2003**, *75*, 49-55.

- 1  
2  
3  
4  
5  
6  
7  
8  
9  
10  
11  
12  
13  
14  
15  
16  
17  
18  
19  
20  
21  
22  
23  
24  
25  
26  
27  
28  
29  
30  
31  
32  
33  
34  
35  
36  
37  
38  
39  
40  
41  
42  
43  
44  
45  
46  
47  
48  
49  
50  
51  
52  
53  
54  
55  
56  
57  
58  
59  
60
- (9) Karrasch, S.; Bullough, P. A.; Ghosh, R. The 8.5 Å Projection Map of the Lightharvesting Complex I from *Rhodospirillum rubrum* Reveals a Ring Composed of 16 Subunits. *EMBO J.* **1995**, *14*, 631-638.
- (10) McDermott, G.; Prince, S. M.; Freer, A. A.; Hawthornthwaitelawless, A. M.; Papiz, M. Z.; Cogdell, R. J.; Isaacs, N. W. Crystal Structure of an Integral Membrane Light-harvesting Complex from Photosynthetic Bacteria. *Nature* **1995**, *374*, 517-521.
- (11) Koepke, J.; Hu, X.; Muenke, C.; Schulten, K.; Michel, H. The Crystal Structure of the Light-harvesting Complex II (B800-850) from *Rhodospirillum molischianum*. *Structure* **1996**, *4*, 581-597.
- (12) Enriquez, M. M.; Akhtar, P.; Zhang, C.; Garab, G.; Lambrev, P. H.; Tan, H.-S. Energy Transfer Dynamics in Trimers and Aggregates of Light-harvesting Complex II Probed by 2D Electronic Spectroscopy. *J. Chem. Phys.* **2015**, *142*, 212432.
- (13) Bricker, W. P.; Shenai, P. M.; Ghosh, A.; Liu, Z.; Enriquez, M. G. M.; Lambrev, P. H.; Tan, H. S.; Lo, C. S.; Tretiak, S.; Fernandez Alberti, S.; Zhao, Y. Non-radiative Relaxation of Photoexcited Chlorophylls: Theoretical and Experimental Study. *Sci. Rep.* **2015**, *5*, 13625.
- (14) Shenai, P. M.; Fernandez-Alberti, S.; Bricker, W. P.; Tretiak, S.; Zhao, Y. Internal Conversion and Vibrational Energy Redistribution in Chlorophyll A. *J. Phys. Chem. B* **2016**, *120*, 49-58.
- (15) Shi, Y.; Liu, J. Y.; Han, K. L. Investigation of the Internal Conversion Time of the Chlorophyll a from S3, S2 to S1. *Chem. Phys. Lett.* **2005**, *410*, 260-263.
- (16) Dong, L. Q.; Niu, K.; Cong, S. L. Theoretical Study of Vibrational Relaxation and Internal Conversion Dynamics of Chlorophyll-a in Ethyl Acetate Solvent in Femtosecond Laser Fields. *Chem. Phys. Lett.* **2006**, *432*, 286-290.
- (17) Dong, L. Q.; Niu, K.; Cong, S. L. Theoretical Analysis of Internal Conversion Pathways and Vibrational Relaxation Process of Chlorophyll-a in Ethyl Ether Solvent. *Chem. Phys. Lett.* **2007**, *440*, 150-154.
- (18) Kosumi, D.; Nakagawa, N.; Sakai, S.; Nagaoka, Y.; Maruta, S.; Sugisaki, M.; Dewa, T.; Nango, M.; Hashimoto, H. Ultrafast Intramolecular Relaxation Dynamics of Mg- and Zn-bacteriochlorophyll a. *J. Chem. Phys.* **2013**, *139*, 034311.
- (19) Musewald, C.; Hartwich, G.; Lossau, H.; Gilch, P.; Pöllinger-Dammer, F.; Scheer, H.; Michel-Beyerle, M. E. Ultrafast Photophysics and Photochemistry of [Ni]-bacteriochlorophyll a. *J. Phys. Chem. B* **1999**, *103*, 7055-7060.
- (20) Kosumi, D.; Maruta, S.; Fujii, R.; Kanemoto, K.; Sugisaki, M.; Hashimoto, H. Ultrafast Excited State Dynamics of Monomeric Bacteriochlorophyll a. *Phys. Status Solidi C* **2011**, *8*, 92-95.
- (21) Nelson, T.; Fernandez-Alberti, S.; Chernyak, V.; Roitberg, A. E.; Tretiak, S. Nonadiabatic Excited-State Molecular Dynamics Modeling of Photoinduced Dynamics in Conjugated Molecules. *J. Phys. Chem. B* **2011**, *115*, 5402-5414.
- (22) Nelson, T.; Fernandez-Alberti, S.; Roitberg, A.; Tretiak, S. Nonadiabatic Excited-State Molecular Dynamics: Modeling Photophysics in Organic Conjugated Materials. *Acc. Chem. Res.* **2014**, *47*, 1155-1164.
- (23) Alfonso Hernandez, L.; Nelson, T.; Tretiak, S.; Fernandez Alberti, S. Photoexcited Energy Transfer in a Weakly Coupled Dimer. *J. Phys. Chem. B*, **2015**, *119*, 7242-7252.

- 1  
2  
3  
4  
5  
6  
7  
8  
9  
10  
11  
12  
13  
14  
15  
16  
17  
18  
19  
20  
21  
22  
23  
24  
25  
26  
27  
28  
29  
30  
31  
32  
33  
34  
35  
36  
37  
38  
39  
40  
41  
42  
43  
44  
45  
46  
47  
48  
49  
50  
51  
52  
53  
54  
55  
56  
57  
58  
59  
60
- (24) Oldani, N.; Tretiak, S.; Bazan, G.; Fernandez-Alberti, S. Modeling of Internal Conversion in Photoexcited Conjugated Molecular Donor Used in Organic Photovoltaics. *Energy Environ. Sci.* **2014**, *7*, 1175-1184.
- (25) Adamska, L.; Nayyar, I.; Chen, H.; Swan, A. K.; Oldani, N.; Fernandez-Alberti, S.; Golder, M. R.; Jasti, R.; Doorn, S. K.; Tretiak, S. Self-Trapping of Excitons, Violation of Condon Approximation, and Efficient Fluorescence in Conjugated Cycloparaphenylenes. *Nano Lett.* **2014**, *14*, 6539-6546.
- (26) Ondarse-Alvarez, D.; Oldani, N.; Tretiak, S.; Fernandez-Alberti, S. Computational Study of Photoexcited Dynamics in Bichromophoric Cross-shaped Oligofluorene. *J. Phys. Chem. A* **2014**, *118*, 10742-10753.
- (27) Tully, J. C. Molecular-Dynamics with Electronic-Transitions. *J. Chem. Phys.* **1990**, *93*, 1061-1071.
- (28) Hammes-Schiffer, S.; Tully, J. C. Proton-Transfer in Solution-Molecular-Dynamics with Quantum Transitions. *J. Chem. Phys.* **1994**, *101*, 4657-4667.
- (29) Tretiak, S.; Mukamel, S. Density Matrix Analysis and Simulation of Electronic Excitations in Conjugated and Aggregated Molecules. *Chem. Rev.* **2002**, *102*, 3171-3212.
- (30) Chernyak, V.; Schulz, M. F.; Mukamel, S.; Tretiak, S.; Tsiper, E. V. Krylov-Space Algorithms for Time-Dependent Hartree-Fock and Density Functional Computations. *J. Chem. Phys.* **2000**, *113*, 36-43.
- (31) Tretiak, S.; Isborn, C. M.; Niklasson, A. M. N.; Challacombe, M. Representation Independent Algorithms for Molecular Response Calculations in Time-Dependent Self-Consistent Field Theories. *J. Chem. Phys.* **2009**, *130*, 054111.
- (32) Furche, F.; Ahlrichs, R. Adiabatic Time-Dependent Density Functional Methods for Excited State Properties. *J. Chem. Phys.* **2002**, *117*, 7433-7447.
- (33) Tretiak, S.; Chernyak, V. Resonant Nonlinear Polarizabilities in the Time-Dependent Density Functional Theory. *J. Chem. Phys.* **2003**, *119*, 8809-8823.
- (34) Tommasini, M.; Chernyak, V.; Mukamel, S. Electronic Density-Matrix Algorithm for Nonadiabatic Couplings in Molecular Dynamics Simulations. *Int. J. Quantum Chem.* **2001**, *85*, 225-238.
- (35) Chernyak, V.; Mukamel, S. Density-Matrix Representation of Nonadiabatic Couplings in Time-Dependent Density Functional (TDDFT) Theories. *J. Chem. Phys.* **2000**, *112*, 3572-3579.
- (36) Send, R.; Furche, F. First-Order Nonadiabatic Couplings from Time-Dependent Hybrid Density Functional Response Theory: Consistent Formalism, Implementation, and Performance. *J. Chem. Phys.* **2010**, *132*, 044107.
- (37) Mukamel, S. Photochemistry-Trees to Trap Photons. *Nature* **1997**, *388*, 425-427.
- (38) Mukamel, S.; Tretiak, S.; Wagersreiter, T.; Chernyak, V. Electronic Coherence and Collective Optical Excitations of Conjugated Molecules. *Science* **1997**, *277*, 781-787.
- (39) Tretiak, S.; Chernyak, V.; Mukamel, S. Recursive Density-Matrix-Spectral-Moment Algorithm for Molecular Nonlinear Polarizabilities. *J. Chem. Phys.* **1996**, *105*, 8914-8928.
- (40) Tretiak, S.; Zhang, W. M.; Chernyak, V.; Mukamel, S. Excitonic Couplings and Electronic Coherence in Bridged Naphthalene Dimers. *Proc. Natl. Acad. Sci. U. S. A.* **1999**, *96*, 13003-13008.

- (41) Dewar, M. J. S.; Zoebisch, E. G.; Healy, E. F.; Stewart, J. J. P. AM1: A New General Purpose Quantum Mechanical Model. *J. Am. Chem. Soc.* **1985**, *107*, 3902-3909.
- (42) Stewart, J. J. P. Optimization of Parameters for Semiempirical Methods IV: Extension of MNDO, AM1, and PM3 to More Main Group Elements. *J. Mol. Model.* **2004**, *10*, 155-164.
- (43) Shavitt, I. *Modern Theoretical Chemistry*; Plenum Press: New York, NY, USA, 1976.
- (44) Szalay, P. G.; Müller, T.; Gidofalvi, G.; Lischka, H.; Shepard, R. Multiconfiguration Self-Consistent Field and Multireference Configuration Interaction Methods and Applications. *Chem. Rev.* **2012**, *112*, 108-181.
- (45) Reynolds, C. H. An AM1 Theoretical Study of the Structure and Electronic Properties of Porphyrin. *J. Org. Chem.* **1988**, *53*, 6061-6064.
- (46) Zandler, M. E.; D'Souza, F. Electronic and Structural Properties of the Metalloporphyrin Structural Isomers: Semiempirical AM1 and PM3 Calculations. *J. Mol. Struct.: THEOCHEM* **1997**, *401*, 301-314.
- (47) Katagi, T. Semi-Empirical AM1 and PM3 Calculations of Five- and Six-Coordinate Oxo Iron (iv) Porphyrin Complexes. *J. Mol. Struct.: THEOCHEM* **2005**, *728*, 49-56.
- (48) Stewart, J. J. P. Optimization of Parameters for Semiempirical Methods I. Method. *J. Comp. Chem.* **1989**, *10*, 209-220.
- (49) Stewart, J. J. P. Optimization of Parameters for Semiempirical Methods II. Applications. *J. Comp. Chem.* **1989**, *10*, 221-264.
- (50) Stewart, J. J. P. Optimization of Parameters for Semiempirical Methods III. Extension of PM3 to Be, Mg, Zn, Ga, Ge, As, Se, Cd, In, Sn, Sb, Te, Hg, Tl, Pb, and Bi. *J. Comp. Chem.* **1991**, *12*, 320-341.
- (51) Linnanto, J.; Korppi-Tommola, J. Spectroscopic Properties of Mg-chlorin, Mg-porphyrin and chlorophylls *a*, *b*, *c1*, *c2*, *c3* and *d* Studied by Semi-Empirical and *ab initio* MO/CI methods. *Phys. Chem. Chem. Phys.* **2000**, *2*, 4962-4970.
- (52) Linnanto, J.; Korppi-Tommola, J. Spectroscopic Properties of Mg-chlorin, Mg-bacterochlorin and Bacteriochlorophylls *a*, *b*, *c*, *d*, *e*, *f*, *g*, and *h* Studied by Semiempirical and *ab initio* MO/CI Methods. *J. Phys. Chem. A* **2001**, *105*, 3855-3866.
- (53) Linnanto, J.; Korppi-Tommola, J. Quantum Chemical Simulation of Excited States of Chlorophylls, Bacteriochlorophylls and Their Complexes. *Phys. Chem. Chem. Phys.* **2006**, *8*, 663-687.
- (54) Nguyen, K. A.; Day, P. N.; Pachter, R.; Tretiak, S.; Chernyak, V.; Mukamel, S. Analysis of Absorption Spectra of Zinc Porphyrin, Zinc *meso*-Tetraphenylporphyrin, and Halogenated Derivatives. *J. Phys. Chem. A* **2002**, *106*, 10285-10293.
- (55) Nelson, T.; Fernandez-Alberti, S.; Chernyak, V.; Roitberg, A. E.; Tretiak, S. Nonadiabatic Excited-State Molecular Dynamics: Numerical Tests of Convergence and Parameters. *J. Chem. Phys.* **2012**, *136*, 054108.
- (56) Wu, C.; Malinin, S. V.; Tretiak, S.; Chernyak, V. Y. Multiscale Modeling of Electronic Excitations in Branched Conjugated Molecules Using an Exciton Scattering Approach. *Phys. Rev. Lett.* **2008**, *100*, 057405.
- (57) Tretiak, S.; Middleton, C.; Chernyak, V.; Mukamel, S. Exciton Hamiltonian for the

- 1 Bacteriochlorophyll System in the LH2  
2 Antenna Complex of Purple Bacteria. *J.*  
3 *Phys. Chem.* **2000**, *104*, 4519-4528.  
4
- 5 (58) Tretiak, S.; Middleton, C.; Chernyak,  
6 V.; Mukamel, S. Bacteriochlorophyll and  
7 Carotenoid Excitonic Couplings in the  
8 LH2 System of Purple Bacteria. *J. Phys.*  
9 *Chem. B* **2000**, *104*, 9540-9553.  
10
- 11 (59) Gouterman, M. Spectra of Porphyrins. *J.*  
12 *Mol. Spectrosc.* **1961**, *6*, 138-163.  
13
- 14 (60) Gouterman, M.; Wagniere, G. H. Spec-  
15 tra of Porphyrins. Part II. Four Orbital  
16 Model. *J. Mol. Spectrosc.* **1963**, *11*, 108-  
17 127.  
18
- 19 (61) Weiss, C. In *The Porphyrins*; Dolphin,  
20 D., Eds.; Academic Press: New York,  
21 1978; Vol. *III*, pp 211-223.  
22
- 23 (62) Kobayashi, M.; Akiyama, M.; Kano, H.;  
24 Kise, H. In *Chlorophylls and Bacteri-*  
25 *ochlorophylls: Biochemistry, Biophysics,*  
26 *Functions and Applications*; Grimm, B.,  
27 Porra, R. J., Rüdiger, W., Scheer, H.,  
28 Eds.; Springer: Dordrecht, The Nether-  
29 lands, 2006; Vol. *25*, pp 79-94.  
30
- 31 (63) Novoderezhkin, V.; Marin, A.; van Gron-  
32 delle, R. Intra- and Inter-Monomeric  
33 Transfers in the Light Harvesting LHCII  
34 Complex: the Redfield-Förster Picture.  
35 *Phys. Chem. Chem. Phys.* **2011**, *13*,  
36 17093-17103.  
37
- 38 (64) Müh, F.; Madjet, M. E.-A.; Renger, T.  
39 Structure-Based Identification of Energy  
40 Sinks in Plant Light-Harvesting Complex  
41 II. *J. Phys. Chem. B* **2010**, *114*, 13517-  
42 13535.  
43
- 44  
45  
46  
47  
48  
49  
50  
51  
52  
53  
54  
55  
56  
57  
58  
59  
60

## Graphical TOC Entry

